Pendellösung Fringes for X-ray Spherical-Wave Diffraction in a Perfect Crystal

By V. V. Aristov and V. I. Polovinkina

Solid State Physics Institute, USSR Academy of Sciences, Moskovskaya Oblast, Chernogolovka 142432, USSR

and A. M. Afanas'ev and V. G. Kohn

I.V. Kurchatov Institute of Atomic Energy, Moscow 123182, USSR

Abstract

The results of experiments in which an anomalous form of the *Pendellösung* fringes has been discovered together with a classical one are presented. The general theory of X-ray spherical-wave diffraction has been constructed taking into account the change of phase relationships for radiation propagating in vacuum. An explanation of the observed experimental results and classification of possible manifestations of the *Pendellösung* effect are given. New data concerning the previously discovered phenomenon of focusing are presented.

1. Introduction

The phase change of incident and diffracted waves propagating in vacuum, *i.e.* from the source to the crystal and from the crystal to the film, are usually neglected in the analysis of X-ray diffraction images of the crystal. In other words, diffraction phenomena in vacuum are disregarded. Such an approximation proves quite justified since in standard experiments the distance from the source to the film is small and the role of the above-mentioned changes in the phase relationships is negligible.

However, it has been shown recently by Afanas'ev & Kohn (1977) that diffraction phenomena in vacuum play, in general, an important role in forming the diffraction pattern on a photoplate. In particular, a focusing occurs for a certain relation between the crystal thickness *t* and the source–film distance *L*. The phenomenon of focusing was first discovered experimentally by Aristov, Polovinkina, Shmyt'ko & Shulakov (1978) and independently somewhat later by Kozmik & Mikhailyuk (1978). A further experimental investigation (Aristov & Polovinkina, 1978) of this phenomenon under the conditions of slight X-ray absorption in a crystal led to the observation of the *Pendellösung* fringes with a structure greatly different from that observed previously.

The present paper is devoted to a more detailed investigation of this problem, namely an analysis of the diffraction-pattern dependence on the value of t/L. In § 2 the experimental topograms of wedge-shaped germanium and silicon crystals, obtained in the experiment with the total source–film distance of about 2 m, are presented. In the thinner part of the wedge the *Pendellösung* fringes, resembling hyperbolae, are bent towards the thick part of the crystal. The interference pattern of this type will be later referred to as *the anomalous Pendellösung effect*.

The general theory of X-ray spherical-wave diffraction is given in § 3. In § 4 new data concerning the phenomenon of focusing are presented. In § 5 a detailed analysis of possible types of *Pendellösung* effect is given.

2. Anomalous *Pendellösung* effect. Experiment

Waves with different refractive indices are excited when X-rays diffract in a perfect crystal. The interference of these waves leads to the crystal beating first predicted by Ewald (1917) and called *the 'Pendellösung'*
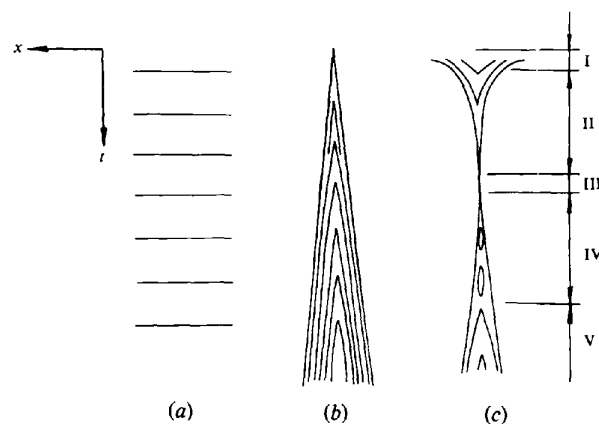

Fig. 1. *Pendellösung* fringes in a perfect crystal. (*a*) Incident plane X-ray wave. (*b*) Incident spherical wave; interference pattern of Kato's type. (*c*) Incident spherical wave; interference pattern obtained in the present paper.

phenomenon. The interference pattern depends on the form of the incident wave. Thus, if the incident wave is plane, the image of a wedge-shaped crystal represents *a series of equidistant interference fringes* (Fig. 1*a*). In the case of an 'incident spherical wave', as shown theoretically in the papers by Kato (1961, 1968) and experimentally by Kato & Lang (1959), and also by Hart & Milne (1968), *the interference fringes have the form of hyperbolae, the vertices of which are directed towards the thin part of the crystal* (Fig. 1*b*). For small source–film distances section topographs, similar to those depicted in Fig. 1(*b*), are observed in the conventional Lang photography geometry.

However, if one takes into account diffraction phenomena in vacuum, *i.e.* the change of phase relationships for a spherical wave propagating from the source to the film, it is evident from physical considerations that *the topographs presented in Figs. 1(a) and 1(b) are the extreme cases, and there must exist a continuous transition from one case to the other.* The theoretical analysis performed in the present paper (see §§ 4 and 5) shows that such a transition is indeed realized when the ratio t/L changes, where t is the crystal thickness and L is the total source–crystal–film distance. In the case of a wedge-shaped specimen it is convenient to consider a value t_s proportional to L (see formula 3.15). Then on the topograph of a wedge-shaped crystal one may single out *five different sections* (*Fig.* 1(*c*), *depending on the relation between* t *and* t_s, *with different physical structure of interference fringes,* namely:

(I) the region in which the approximation of an incident plane wave is valid $(t \ll t_s)$;

(II) the interference region that precedes the focusing $(t < t_s)$;

(III) the region of focusing (interference fringes are absent) $(t \simeq t_s)$;

(IV) the interference region that follows the focusing $(t > t_s)$;

(V) the region of Kato's theory applicability (no dependence on L) $(t \gg t_s)$.

We observed interference effects in these regions experimentally, the scheme being presented in Fig. 2. The Rigaku Denki instrument Microflex with a focus dimension no more than 10 µm was used as a generator of radiation. The characteristic radiation of Cu $K\alpha$, Au $L\alpha$ and Ag $K\alpha$ lines with wavelengths 1·54, 1·27 and 0·559 Å, respectively, were used.
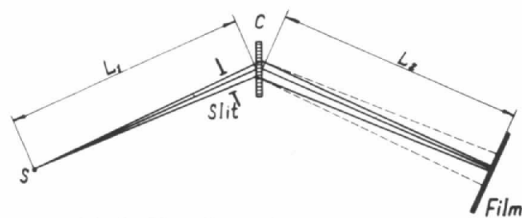
A slit of width 0·5–3 mm was used for singling out a spectral line.

The investigated Ge and Si specimens had the form of a wedge, which permitted us to observe diffraction images forming at different depths of the crystal on the same topograph. The images were developed on MR-type photoplates. To provide a chromatic focusing of the images arising from different sections of the spectral line, a symmetric scheme is used with the source–crystal distance equal to the crystal–film one $(L_1 = L_2)$. The topographs of symmetric Laue
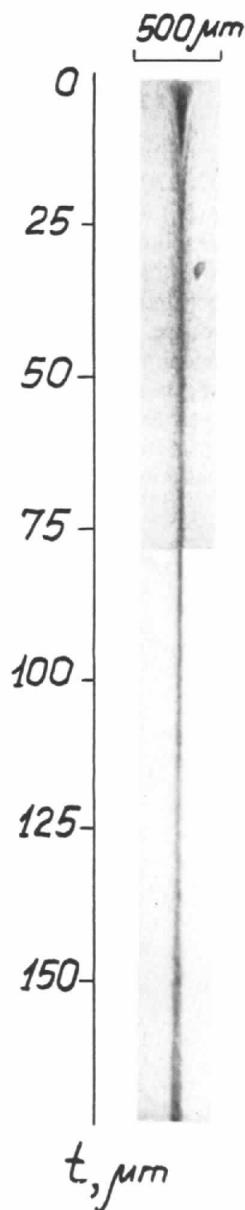

Fig. 3. The topograph of a Si single crystal for large source–film distance ($L = 2 \cdot 3$ m); reflexion 220, radiation Au $L\alpha$ ($\lambda = 1 \cdot 276$ Å).

Fig. 2. The scheme of the experiment.

Table 1. *Values of experimental parameters μ_0, λ, t_s and Λ*

| | | | | | | | | Interference effects observed in different sections of topographs | | | |
No.	Crystal	$h\,k\,l$	λ (Å)	μ_0 (mm^{-1})	L (m)	Λ (μm)	t_s (μm)	I $t \ll t_s$	II $t < t_s$	III $t \simeq t_s$	IV $t > t_s$
1	Ge	1 1 1	1·540	35·4	2·0	8·4	330·1	+	+	−	−
2	Ge	3 3 3	1·540	35·4	2·0	10·6	29·1	−	+	+	−
3	Ge	1 1 1	1·276	21·0	2·3	10·2	380·6	+	+	+	−
4	Ge	3 3 3	1·276	21·0	2·3	14·7	29·0	−	+	+	+
5	Ge	2 2 0	1·276	21·0	2·3	8·2	176·0	+	+	+	−
6	Si	1 1 1	1·276	8·1	1·4	23·3	92·6	+	+	+	+
7	Si	3 3 3	1·276	8·1	2·3	33·8	11·6	−	−	+	+
8	Si	2 2 0	1·276	8·1	2·3	19·2	69·2	−	+	+	+
9	Si	3 1 1	1·276	8·1	2·3	29·1	33·2	−	−	+	+
10	Si	1 1 1	0·559	0·73	1·4	53·6	91·3	−	+	+	+
11	Si	3 3 3	0·559	0·73	1·4	96·7	5·7	−	−	+	+

reflexions 111, 333, 220, 311, at distances $L = 1·4, 2·0, 2·3$ m ($L = L_1 + L_2$) were taken. A diffraction pattern with good linear resolution may be obtained only under conditions of high stability. For this purpose the X-ray generator was operated in the idle regime for 1·5–2 h before the exposure. All possible measures for providing mechanical stability of the set-up were also taken. The time of exposure amounted to 5–20 h.

The general appearance of the image, whose separate sections were observed in different topographs, is shown schematically in Fig. 1(c). In this figure the
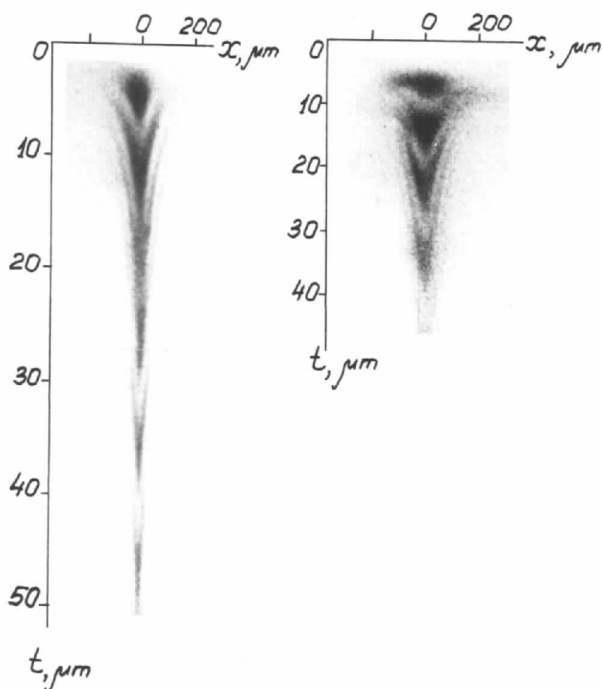

Fig. 4. Experimental patterns of anomalous *Pendellösung* fringes. Fragments of the topographs of a wedge-shaped Ge single crystal at wedge thickness smaller than the thickness of focusing ($t \ll t_s$); $L = 2·3$ m; $\lambda = 1·276$ Å. (a) Reflexion 220; (b) reflexion 111.

regions of the wedge corresponding to the above-mentioned types of interference are also indicated. Character and contrast of interference pattern depend on the relationships between the values of such parameters as the coefficient of X-ray absorption μ_0, the wavelength of radiation λ, the extinction length Λ, and the thickness of focusing t_s.

However, the relationship between these parameters, enabling all the regions I–V to be clearly seen on the same topograph, cannot be realized experimentally. Thus, if $\mu_0 t_s > 2$, the Borrmann effect occurs in regions IV and V and *Pendellösung* fringes are not observed. On the other hand, for $t_s/\Lambda \simeq 1$ there are no *Pendellösung* fringes in regions I and II. Therefore, the experimental parameters μ_0, λ, t_s and Λ were chosen so that different types of interference would be revealed.

In Table 1 the values of these parameters are given for the cases that have been realized experimentally. The regions that were observed in the topograph are also indicated in the table. In Figs. 3–5 the most typical sections of the topographic images obtained are shown. The topograph of a wedge-shaped Si single crystal that corresponds to reflexion 220 for Au $L\alpha$ radiation and $L = 2·3$ m is shown in Fig. 3. In the topograph one can see *the region of focusing* as well as *the region of the anomalous Pendellösung effect* (region II) near the top of the wedge, where the fringes are bent towards the thick part of the crystal.

The *anomalous structure of interference fringes* has been observed in a more distinct form for the case of reflexion from the planes (111) and (220) (Au $L\alpha$ radiation, $L = 2·3$ m) of Ge single crystals. Corresponding topographs are shown in Fig. 4. Near the edge of the wedge (region I) up to 8–10 interference fringes are observed in the direction of the diffraction vector for crystal thickness $t \leq 2\Lambda$. As the crystal thickness increases, the image becomes narrower rapidly and for $t \simeq (4–5)\,\Lambda$ the number of interference fringes diminishes down to one or two

(region II). A specific feature of the topographs is the absence of a sharp boundary of the image in regions I and II.

The interference pattern in a Si single crystal, shown in Fig. 5, for 111 reflexion and $L = 1·4$ m (Ag $K\alpha$ radiation) is displayed in quite another form. Here in the range of thicknesses $t > t_s$ (region IV) *a series of alternating light spots (lagoons) is seen whose form tends to the form of fringes of the classical Pendellösung effect,** as the thickness increases. Let us note that in this region the diffraction pattern already has a sharp boundary (for details see § 5).

Thus, a great variety of interference patterns is observed depending on the conditions of the experiment, each having its specific structure, which naturally provides an opportunity for utilizing interference phenomena in the investigation of crystal structure. In the case of the anomalous *Pendellösung* effect the observed interference pattern contains a great number of fringes, indicating the high resolving power of the method. A thorough theoretical analysis of these problems will be given in § 5.

3. General theory of a spherical-wave diffraction

Let there be a source at point S whose linear dimensions are considered infinitesimal. The scalar field arising from such a source is expressed by the function

$$\psi(\mathbf{r}) = [\exp(i\kappa r)]/r, \qquad (3.1)$$

where r is the distance from the source, and $\kappa = 2\pi/\lambda$.

In such a field the waves with all wave vectors $\mathbf{k}$, whose magnitude is equal to κ, are uniformly distributed. This field may be represented as a two-dimensional Fourier integral with respect to the vectors $\mathbf{q}$ which are perpendicular to an arbitrarily chosen vector $\mathbf{S}_0$ (in the region $\mathbf{S}_0 \mathbf{r} > 0$):

$$\psi(\mathbf{r}) = 2\pi i \int \frac{d\mathbf{q}}{(2\pi)^2} \frac{\exp[i\mathbf{q}\mathbf{r} + i\mathbf{S}_0 \mathbf{r}(\kappa^2 - q^2)^{1/2}]}{(\kappa^2 - q^2)^{1/2}}. \quad (3.2)$$

It is convenient to choose the unit vector corresponding to the exact Bragg direction as $\mathbf{S}_0$.

The components of field for which the Bragg condition holds rather accurately take part effectively in the diffraction process. Therefore, in (3.2) only the components with the wave vectors

$$q \leq |\chi_h|\kappa \qquad (3.3)$$

are of importance.

The Fourier component of the crystal polarizability is known to be rather small, of the order of 10^{-5}–10^{-6}. For this reason it seems quite reasonable to neglect in (3.2) the terms of the order of q^2/κ^2 and substitute $(\kappa^2 - q^2)^{1/2}$ by κ.

---

* Obtained in Lang's conventional scheme of topography.

In fact, an approximation of this type was used by Kato (1961, 1968) for the construction of his spherical-wave diffraction theory. In this approximation the distance from the source to the crystal does not enter the expression for the intensity at all. Thus, the problem was reduced to the determination of wave fields in a crystal in the limiting case, when the source–crystal
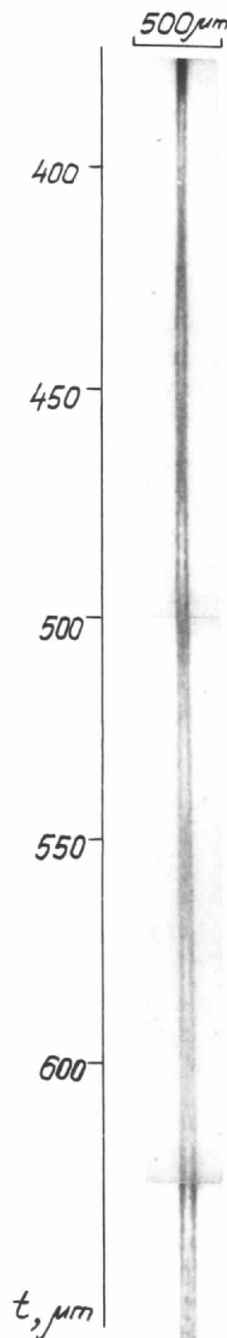

Fig. 5. Wave-field interference at wedge thickness $t > t_s$. A fragment of a Si single-crystal topograph; reflexion 111, $L = 1·4$ m, Ag $K\alpha$ ($\lambda = 0·559$ Å).

distance did not affect the diffraction-pattern character.

In practice, neglecting the terms q^2/κ^2 in the integrand of (3.2) is not always correct. Generally speaking, terms of the order of q^2/κ^2 in the exponent argument should be kept, *i.e.* their smallness may be compensated to a great degree by a large value of $S_0 r = L_1$, where L_1 is the distance from the source to the crystal. Therefore, we shall use the following representation for the electric vector of radiation incident on the crystal:

$$\mathbf{E}^{(in)}(\mathbf{r}) = \frac{2\pi i}{\kappa} \int \frac{d\mathbf{q}}{(2\pi)^2} \exp[i\mathbf{k}_0(\mathbf{q})\mathbf{r}] \sum_s A_s \mathbf{e}_{0s}, \quad (3.4)$$

where

$$\mathbf{k}_0(\mathbf{q}) = \left(\kappa - \frac{q^2}{2\kappa}\right)\mathbf{S}_0 + \mathbf{q}, \quad s = \pi, \sigma. \quad (3.5)$$

The polarization vectors $\mathbf{e}_{0s}$ in general also depend on $\mathbf{q}$, but this dependence may be neglected in the region (3.3). We choose the vector $\mathbf{e}_{0s}$ in the form

$$\mathbf{e}_{0\sigma} = \frac{\boldsymbol{\sigma}}{|\boldsymbol{\sigma}|}, \quad \boldsymbol{\sigma} = [\mathbf{S}_0 \times \mathbf{h}], \quad \mathbf{e}_{0\pi} = [\mathbf{e}_{0\sigma} \times \mathbf{S}_0], \quad (3.6)$$

where $\mathbf{h}$ is the reciprocal-lattice vector multiplied by 2π.

In (3.4) we take into account some change of the wave-vector projection in the direction $\mathbf{S}_0$ for the waves incident on the crystal in the off-Bragg direction. Despite the fact that this change has rather a small value, $\Delta k = q^2/2\kappa$, it may result in a noticeable wave phase change at the entrance surface of the crystal. This may eventually lead to an essential rearrangement of the diffraction pattern as a whole. The field distribution near a crystal surface corresponding to approximation (3.4) is determined by an expression of the form

$$\mathbf{E}^{(in)}(\mathbf{r}) \simeq \frac{1}{L_1} \exp\left[i\boldsymbol{\kappa}_0 \mathbf{r} + \frac{i\kappa}{L_1}\rho^2\right] \sum_s A_s \mathbf{e}_{0s}, \quad (3.7)$$

where $\boldsymbol{\kappa}_0 = \kappa \mathbf{S}_0$, $\rho = \mathbf{r} - \mathbf{S}_0 L_1$ is the vector in the plane perpendicular to $\mathbf{S}_0$. Formula (3.7) is a standard representation of a spherical wave at a great distance from the source.

Given the expansion of the incident wave with respect to plane waves, the wave field in the crystal and behind it is found in accordance with a standard procedure. The plane wave with the wave vector $\mathbf{k}_0$ and a unit amplitude diffracting in the crystal is reflected and transformed into the plane wave with the wave vector

$$\mathbf{k}_h = \mathbf{k}_0 + \mathbf{h} - \alpha \mathbf{n}_0/2, \quad (3.8)$$

where $\mathbf{n}_0$ is the unit vector of the normal to the entrance surface of the crystal, and the parameter α is deter-

mined from the condition $\mathbf{k}_h^2 = \mathbf{k}_0^2 = (2\pi/\lambda)^2$. Below, we confine ourselves to the case of the vectors $\mathbf{k}_0$ and $\mathbf{k}_h$ making equal angles with the surface of the crystal. In this case the parameter α is determined, with an accuracy of up to q^2/κ^2, by the expression

$$\alpha = \alpha_1 + \alpha_2, \quad \alpha_1 = \frac{2\mathbf{h}\mathbf{q}}{\kappa\gamma_0}, \quad \alpha_2 = \frac{q^2(1 - \cos 2\theta_B)}{\kappa\gamma_0}, \quad (3.9)$$

where $\gamma_0 = \mathbf{S}_0 \mathbf{n}_0$, θ_B is the Bragg angle. The amplitude of a reflected plane wave is known (see *e.g.* Pinsker, 1978):

$$R_s(\alpha_1 t) = \left(\frac{\chi_h}{\chi_{\bar{h}}}\right)^{1/2} \sum_j \frac{z_j}{2(1 + y^2)^{1/2}} \exp[-\mu_{sj} t/2]$$

$$\times \exp[i(\varepsilon_{sj} + \alpha_1)t/2], \quad (3.10)$$

where

$$\varepsilon_{sj} = \frac{\kappa}{\gamma_0}[\chi_{r0} - |\chi_{rh}|C_s(y - z_j(1 + y^2)^{1/2})],$$

$$\mu_{sj} = \frac{\mu_0}{\gamma_0}\left[1 - z_j C_s \frac{\varepsilon_h}{(1 + y^2)^{1/2}}\right],$$

$$\varepsilon_h = \frac{|\chi_{ih}|}{|\chi_{i0}|}, \quad y = \frac{\alpha_1 \gamma_0}{2\kappa|\chi_{rh}|C_s} \quad (3.11)$$

$$z_j = \begin{cases} +1 & j = 1 \\ -1 & j = 2 \end{cases}$$

$$C_s = \begin{cases} 1 & s = \sigma \\ \cos 2\theta_B & s = \pi. \end{cases}$$

Here, $\chi = \chi_r + i\chi_i$ is the complex polarizability of the crystal and χ_0 and χ_h are the null and the hth Fourier components, t is the thickness of a crystal plate.

As a result, the amplitude of the electric field of a diffracted spherical wave behind the crystal takes the form

$$\mathbf{E}_h^{(out)}(\mathbf{r}) = \sum_s A_s \mathbf{e}_{hs} \frac{2\pi i}{\kappa} \int \frac{d\mathbf{q}}{(2\pi)^2} R_s(\mathbf{q}, t)$$

$$\times \exp[i\mathbf{k}_0(\mathbf{q})\mathbf{r}_0 + i\mathbf{k}_h(\mathbf{q})(\mathbf{r} - \mathbf{r}_0)], \quad (3.12)$$

where $\mathbf{e}_{hs}$ are the polarization vectors in the plane perpendicular to $\mathbf{S}_h = \mathbf{S}_0 + \mathbf{h}/\kappa$. They are determined by formulae (3.6), in which $\mathbf{S}_0$ should be substituted by $\mathbf{S}_h$. Vector $\mathbf{r}_0$ is the distance from the source to the entrance surface of the crystal. It is easy to see that the integral (3.12) will be of a noticeable value only in the case of the vector $\mathbf{r}_0$ parallel to $\mathbf{S}_0$ and the vector $(\mathbf{r} - \mathbf{r}_0)$ directed closely to $\mathbf{S}_h$. We put a screen (film) perpendicular to $\mathbf{S}_h$ and let ρ be a vector in the plane of the screen. Of greatest interest is an experiment in

which a crystal is halfway between the source and the detector. In this case

$$\mathbf{r}_0 = \mathbf{S}_0 L/2 \quad \mathbf{r} = \mathbf{r}_0 + \mathbf{n}_0 t + \mathbf{S}_h L/2 + \mathbf{p}.$$

For the sake of simplicity let us assume that the vector $\mathbf{n}_0$ lies in the scattering plane, *i.e.* in the plane of the vectors $\mathbf{S}_0$ and $\mathbf{S}_h$. Then the integration in the direction normal to this plane leads again to an expression of type (3.7) as a factor, while it is convenient to express the remaining integral in terms of y. As a result, we obtain the expression for the intensity in the reflected beam:

$$I_h(x) = \frac{1}{2L} \sum_s G_s \left| \sum_j \int \mathrm{d}y F_{sj}(y) \exp \left| i\varphi_{sj}(x, y) \right| \right|^2, \quad (3.13)$$

where

$$F_{sj}(y) = \frac{z_j}{2(1 + y^2)^{1/2}} \exp \left[-\frac{\mu_{sj} t}{2} \right], \quad G_s = \frac{|\chi_{rh}|^2 C_s^2}{\lambda \sin^2 2\theta_B}$$

$$\varphi_{sj}(x, y) = \frac{\pi t}{A_s} \left[py + z_j(1 + y^2)^{1/2} - \frac{1}{2} q_s y^2 \right]. \quad (3.14)$$

Here x is the projection of $\mathbf{p}$ in the direction of $\mathbf{p}_{h\tau}$. The intensity is independent of the coordinate in the perpendicular direction.

$$p = x/t \sin \theta_B, \quad q_s = t_s/t,$$

$$t_s = \frac{\lambda L}{2A_s \sin^2 \theta_B}, \quad A_s = \frac{\lambda \cos \theta_B}{|\chi_{rh}| C_s}. \quad (3.15)$$

In (3.13) the incident radiation is supposed to be unpolarized and the crystal to consist of atoms of the same kind.

Formulae (3.13)–(3.15) are the basis for the calculation of a diffraction pattern. A concrete analysis of these formulae will be given in the following sections. Here we only mention that the variety of interference patterns considered in the previous section is due to the appearance of a new phase term in the integrand. This term is proportional to $q_s = t_s/t$. If one sets $q_s = 0$ (3.13) will exactly correspond to the result obtained by Kato (1961, 1968). The new parameter t_s determines the thickness of the crystal, focusing a wave field at a distance L from the source.

4. Diffraction focusing of a spherical wave

If the crystal thickness t (or the focusing thickness t_s) is much greater than the extinction length A, the integrand phase in (3.13), as seen from (3.14), will change very rapidly with y. Therefore, the value of the integral will be much smaller than $|F|Ay$ due to strong oscillations of the integrand, where Ay is the characteristic interval in which the integrand modulus noticeably differs from zero. It is most convenient to

perform an analysis of the problem in this case by the method of stationary phase (Jeffreys & Swirles, 1966). According to this method the region near the point y_0 at which $\partial\varphi/\partial y = 0$ makes the main contribution to the integral. The contribution is determined by the value of the integrand at this point and by the value of the second derivative of the phase $\partial^2\varphi/\partial y^2$.

As a result, one may obtain for $I_h(x)$ the approximate expression

$$I_h(x) \simeq \frac{1}{2L^2} \sum_s \left| \sum_j \frac{F_{sj}(y_0)}{\left[1 - \frac{z_j}{q_s(1 + y_0^2)^{3/2}} \right]^{1/2}} \right. $$
$$\left. \times \exp \left[i\varphi_{sj}(y_0) \right] \right|^2. \quad (4.1)$$

Only one stationary point, y_0, is supposed to exist on each sheet of the dispersion surface. We remark that the value y_0 depends on x, t, L, as well as on the indices s and j. By differentiation of (3.14) it is easy to obtain the equations for determining y_0, namely:

$$p + z_j \frac{y_0}{(1 + y_0^2)^{1/2}} - q_s y_0 = 0. \quad (4.2)$$

In particular, it follows from this equation that any value of y can be stationary. Moreover, if one chooses a certain value of y, (4.2) will immediately determine the coordinate $x = pt \sin \theta_B$ at which this value will be stationary for the given q. We proceed to take (4.1) into account. It is easy to see that for every value of y_0 for $z_j = 1$ (slightly absorbed mode) the square root in the denominator vanishes if

$$q_s = \frac{1}{(1 + y_0^2)^{3/2}}. \quad (4.3)$$

In this case, (4.1) diverges. Physical interpretation of this divergence is based on the effect of focusing of an X-ray spherical wave. Integral (3.13) for these values of the parameters has a sharp maximum. The determination of its value and structure requires additional information concerning the behaviour of the phase and the modulus of the integrand in the focusing region of angles $y \simeq y_0$.

According to (4.3), the stationary points corresponding to the focus for given t are

$$y_0 = \mp \left[(t/t_s)^{2/3} - 1 \right]^{1/2}. \quad (4.4)$$

Thus, for $t < t_s$ there is no focusing, for $t = t_s$ the central region of angles near $y_0 = 0$ is focused, and for $t > t_s$ two symmetric off-Bragg regions of angles are focused. It is evident that the strongest maximum should be expected for t slightly exceeding t_s, when the focusing regions of angles, corresponding to the points $\pm y_0$, are still overlapped. Nevertheless, the parameter t_s determines a scale of thickness for which the central

region of angles corresponding to the main maximum is focused.

Substituting (4.4) in (4.2), it is easy to obtain a locus of foci on the plane x, t

$$x_{\pm} = \pm t [1 - (t_s/t)^{2/3}]^{3/2} \sin \theta_B. \qquad (4.5)$$

In the limit $t \gg t_s$ the lines $x = x_{\pm}(t)$ correspond to the edges of the Borrmann fan. However, for all finite t they are inside it.

In the case of a slightly absorbing crystal, focusing on the lines $x = x_{\pm}(t)$ in the region $t > t_s$ leads to the formation of a sharp boundary near the diffraction fringe since in the region $x > x_{\pm}(t)$ the intensity is extremely low (see the next section). This result is in good agreement with the experimental pattern presented in Fig. 5. For $t = 550$ µm, the width of the experimental fringe, Δ_{exp}, is 76 µm. The theoretical estimate following the formula $\Delta_{th} = x_+ - x_-$ gives the value 57 µm ($t_s = 91 \cdot 3$ µm, $\sin \theta_B = 0 \cdot 0893$), whereas the Borrmann fan is 98 µm in this case.

In a strongly absorbing crystal, $\mu_0 t \gg 1$, the Borrmann effect occurs and only the weakly absorbed field is of importance. Therefore, the effective region of integration in (3.13) is small. In this case one may obtain an approximate value of the integral expanding the dependence of μ_{sj} and φ_{sj} on y in a power series and neglecting all the terms of higher order than y^4. As a result, by performing simple calculations we obtain (Afanas'ev & Kohn, 1977):

$$I_h(x) \simeq \frac{1}{2L^2} \sum_s \frac{B_s}{x_{0s}} \exp[-\mu_{as} t] \exp\left[-\frac{x^2}{2x_{0s}^2}\right], \quad (4.6)$$

where

$$B_s = \frac{1}{8} \sqrt{q_s} \, Y_s t_s \sin \theta_B, \quad \mu_{as} = \frac{\mu_0}{\cos \theta_B} (1 - C_s \varepsilon_h),$$

$$x_{0s} = \frac{\Delta}{2} \left[\frac{(q_s - 1)^2 + Q^2}{q_s Q^2}\right]^{1/2}, \quad Q = \frac{2\Delta_s}{\pi t_s} \frac{1}{Y_s^2}, \qquad (4.7)$$

$$Y_s = \left(\frac{4 \cos \theta_B}{\mu_0 t_s C_s \varepsilon_h}\right)^{1/2}, \qquad (4.8)$$

$$\Delta = \frac{2\Delta_s \sin \theta_B}{\pi Y_s}. \qquad (4.9)$$

The parameter Y_s is the effective halfwidth of the integration range in (3.13) for $t = t_s$. According to (4.6) the distribution of intensity in the reflected fringe has a Gaussian form for all thicknesses. The narrowest and highest peak arises for $t = t_s$. The width of the fringe (at height $0 \cdot 6 \, I_{max}$) is equal to Δ in this case, and does not depend on the polarization of the incident radiation.

If the condition $\mu_0 t_s \gg 1$ does not hold, (4.6) is wrong, and (4.9) gives an underestimated value, since

in the limit of $\mu_0 \to 0$, $\Delta = 0$ according to (4.9). However, an approximate value for the width of focus may also be obtained in this limiting case. For this one should determine an effective interval of y values in integral (3.13), in which the phase remains almost constant for $t = t_s$ and $x = 0$. Outside this interval the integrand strongly oscillates and the contribution of these regions to the integral may be neglected. While keeping a term proportional to y^4 in phase φ (3.14), we obtain

$$Y_s = \frac{1}{1 \cdot 2} \left(\frac{8\Delta_s}{\pi t_s}\right)^{1/4} \qquad (4.10)$$

Thus, for a slightly absorbing crystal the focus width is determined by (4.9), in which Y_s should be chosen according to (4.10). In this case the parameter Δ depends on the X-ray polarization. In the general case it is necessary to choose the minimum value among the two values (4.8) and (4.10). If these values are close, a slightly smaller value for Y_s should be chosen.

The experimental curve $I(x)$ obtained by the photometry of a reflected fringe in the field of focusing ($t \simeq t_s$) is shown in Fig. 6(a) for the case Ge, Au Lα, 220. For comparison the results of the exact calculation of integral (3.13) for this case are presented in Fig. 6(b). The method of calculation is described by Kohn (1979). As seen from the figure, the experimental width of the focus (~18 µm) considerably exceeds the theoretical one ($3 \cdot 5$ µm). The reasons for such disagreement are firstly the finite dimensions of the X-ray tube focus and secondly insufficient mechanical stability of the experimental set-up. Moreover, the orientation of the entrance surface of the specimen was not completely symmetric. Although the deviation from the symmetric position is only 1–2°, it may lead to a considerable broadening of the reflected fringe due to incomplete chromatic focusing. The estimation of the focus width using (4.9) and (4.10) gives for Δ the value $3 \cdot 4$ µm, which is in good agreement with the exact calculation.
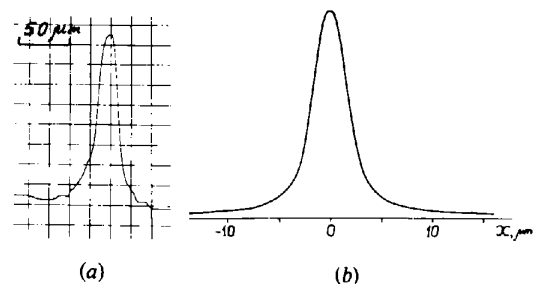

Fig. 6. Ge single-crystal topograph profiles in the region of focusing ($t \simeq t_s$); reflexion 220, $L = 2 \cdot 3$ m, $\lambda = 1 \cdot 276$ Å. (a) Photometric curve; (b) calculated profile in the approximation of a point source.

5. The anomalous *Pendellösung* effect. Theory

Now we proceed to a systematic analysis of the different types of interference patterns arising as the ratio t/t_s changes. First of all, we consider region I (see § 2), when the crystal thickness t is much smaller than t_s. It is necessary for *Pendellösung* fringe observation in this field that t should be greater than Λ. Therefore, the condition $t_s \gg \Lambda$ should also be satisfied or, taking into account (3.15),

$$\lambda L \gg 2(\Lambda \sin \theta_B)^2. \qquad (5.1)$$

In this case an approximate expression for the intensity may be obtained from (4.1) by considering the smallness of the parameter $1/q$. We therefore substitute the square root in the denominator of (4.1) by unity and neglect the second term on the left-hand side of (4.2) when calculating the point of stationary phase. As a result we obtain

$$I_h(x) \simeq \frac{1}{2L^2} \sum_s \left| \sum_j F_{sj}(y_0) \exp[i\varphi_{sj}(y_0)] \right|^2, \qquad (5.2)$$

$$y_0 = \frac{p}{q_s} = \frac{x}{x_s} = \frac{\sin 2\theta_B}{|\chi_{rh}|C_s} \frac{x}{L}, \quad x_s = t_s \sin \theta_B. \qquad (5.3)$$

Formulae (5.2), (5.3) exactly correspond to the results of the dynamical theory of diffraction in the approximation of an incident plane wave, the ratio x/L playing the role of the angular variable. Thus, the intensity at the point x is approximately determined by a plane-wave component in the expansion of a spherical wave corresponding to the angular deflection from the Bragg direction, from which this point is seen at a distance L from the imaginary source. One may say that in this case the reflecting planes of the crystal are similar to a mirror with an extremely high sensitivity to the incidence angle, *i.e.* only the rays close to the Bragg direction are reflected.

Taking into account (3.11) and (3.14), we may rewrite (5.2) in the form

$$I_h(x) = \frac{1}{2L^2} \exp\left[-\frac{\mu_0 t}{\gamma_0} \right]$$

$$\times \sum_s \frac{\tilde{A}_s^2(x)}{A_s^2} \left| \sin\left(\frac{\pi t}{\tilde{A}_s(x)} - i\frac{\tilde{\mu}_s t}{2\gamma_0} \right) \right|^2, \qquad (5.4)$$

where

$$\tilde{\mu}_s = \mu_0 C_s \varepsilon_h \tilde{A}_s(x)/A_s, \qquad (5.5)$$

$$\tilde{A}_s(x) = \frac{A_s}{|1 + (x/x_s)^2|^{1/2}}. \qquad (5.6)$$

As immediately seen from (5.4), in the case of a slightly absorbing crystal, $\mu_0 t \ll 1$, the intensity oscillates with the increase in t, but the period of oscillation depends on x. For $x = 0$ the period has a

maximum and diminishes as $|x|$ increases. Consequently, the dark and light fringes (*Pendellösung* fringes) will have a narrower spacing at the edges of the diffraction region and a wider spacing in the centre, *i.e.* on the line $x = 0$. Therefore, the central part of the fringe turns out to be bent towards the thick part of the wedge.

The degree of bending of the fringes depends on L. In the limit $L \to \infty$ the fringes are straight, which corresponds to the plane-wave incidence at the Bragg angle (see Fig. 1a). In practice, the fringes are always bent due to L finiteness, and the first fringe broadens out in the centre. The length of a linear section is of the order of $x_s (\Lambda_s/t)^{1/2}$.

With the increase in crystal thickness, approximation (5.4) proves insufficient as a description of the anomalous *Pendellösung* effect. In this region (region II) it is necessary to use more general formulae (4.1), (4.2). Then, even in a slightly absorbing crystal, the relationship between the amplitudes of interfering waves changes, which leads to weakening in the contrast of the interference pattern. Besides, the phase relationships change because the stationary phase points for the two waves become different (see Fig. 8a).

In order to comprehend specific properties of the arising changes, we consider the central part of the interference pattern corresponding to small values of x. In this case the roots of (4.2) are approximately

$$y_{0j} \simeq \frac{p}{(q_s - z_j)}. \qquad (5.7)$$

Substituting these values in (3.14), we calculate the phase difference of two interfering waves in the form of a power series in x; keeping only the first two terms, we obtain

$$\Delta\varphi = \frac{2\pi t}{\Lambda_s} \left[1 + \frac{1}{2} \frac{x^2}{(t_s^2 - t^2)\sin^2 \theta_B} + \dots \right]. \qquad (5.8)$$

When $t \ll t_s$, the phase difference changes with the increase in x according to (5.6). However, with the increase in t the change of the phase difference becomes more rapid, and the length of a linear section shortens and vanishes when t tends to t_s. Thus, the interference fringes are more strongly bent towards the focus region.

Such a character of the interference pattern is clearly seen in the experimental topograph of the acute part of the Ge wedge in the case of 111 reflexion (see Fig. 4b). Here the condition $t_s \gg \Lambda$ (see Table 1) is satisfied and, besides, the polarization factor, $\cos 2\theta_B$ is close to unity. In the topograph, V shaping of the fringes with the increase in t and worsening of the contrast are seen. The latter is connected with a relatively high absorption coefficient, and consequently with the Borrmann effect for one of waves, but not with focusing, since the intensity averaged over the period of oscillations

decreases with the increase of t. In the case of the 220 reflexion, presented in Fig. 4(a), of interest is a break-down of oscillations because of the difference of Λ_s for the waves with two polarizations. Here it is also clearly seen that the fringes become more acute in the thicker part of the wedge.

In Fig. 7, the theoretical topographs for the two cases, calculated by means of a computer using (4.1) and (4.2), are presented. The calculated topographs are visually broader than the experimental ones due to a different choice of scales along the axes x and t or, in other words, they correspond to a more obtuse wedge. For the rest, it is easy to notice a complete agreement between the experimental results and the theory.

Now we consider the range of thicknesses $t > t_s$. In this region the parameter $q < 1$. We suppose at first that $q \ll 1$ (the Kato case). In this case one may neglect the last term on the left-hand side of (4.2), when calculating the point of stationary phase. The solution (4.2) takes the form:

$$y_{0j} = z_j \frac{p}{(1-p^2)^{1/2}} = z_j \frac{x}{(x_m^2 - x^2)^{1/2}}, \quad x_m = t \sin \theta_B.$$
$$(5.9)$$

It follows from (5.9) that the points of stationary phase exist only in the region $|p| < 1$ or $|x| < x_m$, which is usually called the 'Borrmann fan'. According to the Kato theory, reflexion of X-rays in a crystal occurs only in this region, which completely determines the width of the reflected beam. As known from the generalized dynamical theory (Pinsker, 1978), such a result is obtained strictly only in the case of the δ-function character of field distribution on the entrance surface of a crystal. From this viewpoint the Kato theory describes the situation when the source of the spherical wave is located just in front of the crystal. In fact, the result (5.9), being approximate, proves to hold also in the case of the source at some distance from the crystal, provided that $t \gg t_s$.

When calculating the intensity in this extreme case, we may neglect unity compared with the second term of the square root in the denominator. Taking into account (5.9), we have

$$I_h(x) = \frac{1}{2L^2} \exp\left[-\frac{\mu_0 t}{\gamma_0}\right]$$
$$\times \sum_s \frac{t_s \tilde{\Lambda}_s^2(x)}{t \Lambda_s^2} \left| \sin\left(\frac{\pi t}{\tilde{\Lambda}_s(x)} + \frac{\pi}{4} - i \frac{\tilde{\mu}_s t}{2\gamma_0}\right)\right|^2, \tag{5.10}$$

where now

$$\tilde{\Lambda}_s(x) = \frac{\Lambda_s}{[1 - (x/x_m)^2]^{1/2}} \tag{5.11}$$

and $\tilde{\mu}_s$ is defined by (5.5) as before. The formula (5.10) differs from (5.4) mainly by the dependence of an effective extinction length on x. According to (5.10), the value of $\tilde{\Lambda}_s(x)$ increases with increase in x, but this means that the fringes are bent towards the thick part of the crystal. Such an interference pattern is usually observed in section topographs. Therefore, the *Pendellösung* effect of such a type, as distinct from (5.4), may be regarded as a classical one.

A remark should be made in connection with (5.10). In the case $q = 0$, integral (3.13) is known to be calculated exactly and expressed in terms of the Bessel function (*e.g.* Afanas'ev & Kohn, 1977; Kato, 1961, 1968). One may be directly convinced that (5.10) is obtained from the exact formula if one uses the asymptotic expansion for the Bessel function at large values of argument $\pi t/\tilde{\Lambda}_s(x)$. Near the edges of the 'Borrmann fan' $x_m - |x| \ll x_m$, where the argument is small, (5.10) is not valid. It should be noted that the exact formula is also not valid in this region, since y_0 becomes large and the term qy_0 in the left-hand side of (4.2) may not be neglected. On the other hand, invalidity of (5.10) is also connected with its divergence for the case of a non-absorbing crystal, which indicates the existence of a specific wave-field focusing (see § 4).

This problem will be discussed later, but now we consider an additional term $\pi/4$ in the sine argument (in 5.10). At the point $x = 0$ the periods of oscillations in crystal thickness are the same and equal to Λ_s in the regions $t \ll t_s$ and $t \gg t_s$. However, the positions of maxima and minima in the region $t \gg t_s$ are shifted with respect to the region $t \ll t_s$ by a quarter of the period. This is connected with the phase change of a slightly absorbing mode ($j = 1$), when it crosses over the focus, where the second derivative equals zero. This effect is well known in optics of visible light (Born & Wolf, 1964).

Now we consider region IV when $t > t_s$, but the parameter $q = t_s/t$ may not be neglected. In this region (4.2) should be solved exactly. Since this equation is equivalent to the fourth-power equation with respect to y_0 its analytic solution is rather cumbersome. The
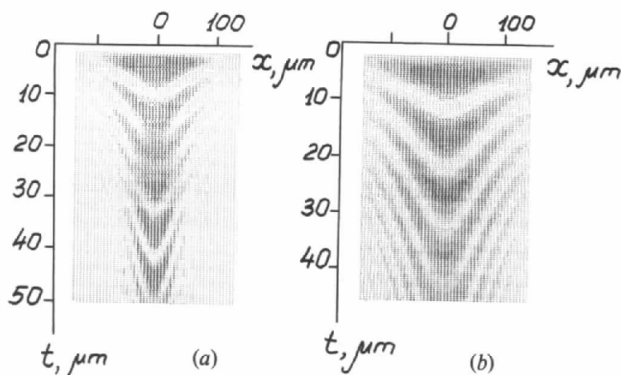

Fig. 7. Theoretical patterns of the anomalous *Pendellösung* effect as calculated using (4.1) for the values of parameters corresponding to the experimental pattern in Fig. 4.

position of the points of stationary phase may be clarified if we solve (4.2) graphically. For this purpose we plot the functions

$$\psi_j(y) = \sin \theta_B \left[t_s - t \frac{z_j}{(1 + y^2)^{1/2}} \right] y, \quad j = 1, 2, \quad (5.12)$$

and draw a line parallel to the abscissa at a distance x from it (see Fig. 8). The points of stationary phase y_0 are intersections of the straight line with the curves.

The physical sense of the points of stationary phase is that they determine the excitement points on the dispersion curve, in the vicinity of which the wave makes a maximum contribution to the point x of the diffraction pattern. Corresponding plane-wave components in the expansion of a spherical wave interfere with one another, the character of interference depending essentially on the phase difference between them. Therefore, these plane waves may be called interference waves, and the corresponding points of excitation on the dispersion surface interference points of excitation or simply interference points.

When $q_s > 1$ both the functions increase monotonically, therefore, for all x the interference points on both sheets of the dispersion surface are on the same side relative to the centre (see Fig. 8a). In the case of $q_s = 1$ the function $\psi_1(y)$ has an inflection point at $y = 0$ (see Fig. 8b), i.e. at this point the function itself and its first and second derivatives with respect to y are equal to zero. Therefore, at the point $x = 0$ we have good focusing in this case.

The situation for $q_s < 1$ is represented in Fig. 8(c). As seen from the figure, the function $\psi_1(y)$ has two extremal points: a maximum and a minimum, with their coordinates defined by (4.4) and the corresponding values by (4.5).

In the region $x_- < x < x_+$ on the dispersion surface, corresponding to slightly absorbed field, there are three interference points at once; therefore, the interference of waves excited from one sheet of the dispersion surface is possible along with an ordinary interference.

Of greatest interest are the interference points corresponding to small values of $|y_0|$ since the amplitude of the interfering wave is small when the opposite is the case. It is necessary to take into account the slope of the curve ψ_j at the point of intersection which determines the spherical-wave angular-component distribution density along the axis x (see Fig. 8b). Indeed, if Δx is a small interval on the axis x, and Δy is a small interval of normalized angles corresponding to Δx, then

$$\frac{\Delta y}{\Delta x} = \frac{1}{|\partial \psi_j / \partial y|}. \quad (5.13)$$

In the method of stationary phase the value of (5.13) enters the intensity expression as a factor.

So, in this case, one may qualitatively analyse the

character of the interference pattern using Fig. 8(c). First of all, it should be mentioned that the slightly absorbed field makes the principal contribution to the total intensity, since for this field the value of (5.13)
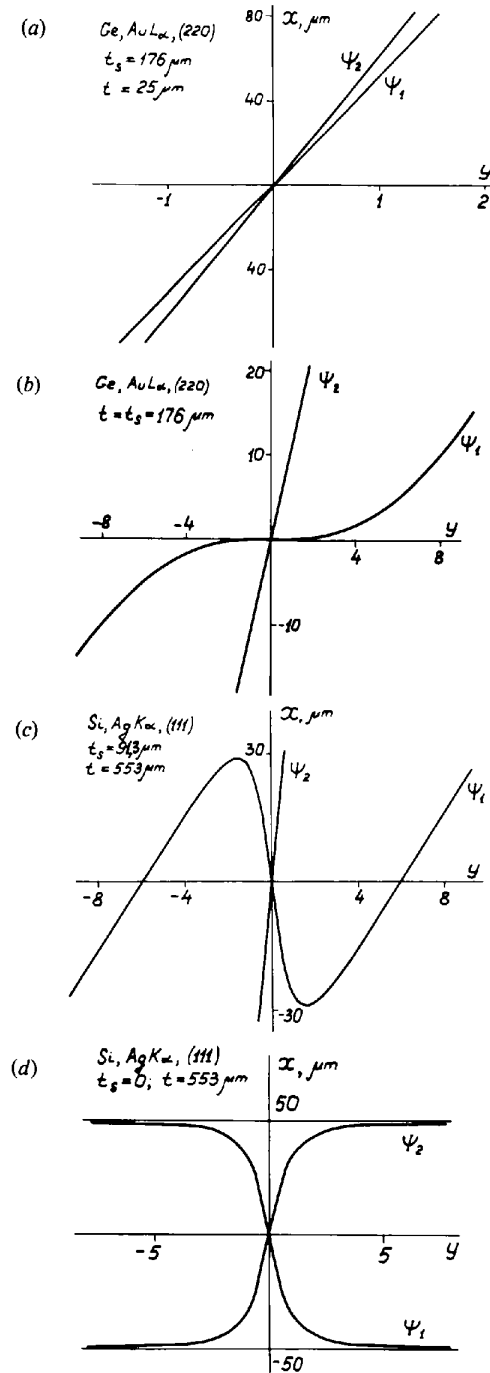

Fig. 8. Curves for graphical determination of interference points on the dispersion surface (stationary phase points). The values of parameters correspond to different types of wave-field interference observed in experiment: (a) the prefocusing anomalous Pendellösung effect ($t < t_s$); (b) focusing ($t = t_s$); (c) interference for $t > t_s$; (d) Kato's case ($t \gg t_s$).

exceeds that for a strongly absorbed field. Besides, this factor increases with increase of $|x|$. At the points $|x| = |x_\pm|$ the radiation is focused, although to a lesser extent than in the case $t = t_s$. In the region $|x| > |x_\pm|$ the intensity of the reflected beam is much lower than in the region $|x| \lesssim |x_\pm|$, since it is formed only by two weak waves unlike the case of the central region, where four waves interfere simultaneously.

The period of oscillations along the axis x is mainly determined by the change of phase difference of interfering waves with the increase of x. According to Fig. 8(c) the interference of waves belonging to the same branch of the dispersion surface (the waves corresponding to the interference points closest to the focus are the most essential) leads to oscillations, with a period much less than that for the waves belonging to different branches. These peculiar oscillations are superimposed on the oscillations corresponding to the interference of waves belonging to different branches of the dispersion surface and the resultant interference pattern proves sufficiently complicated. To observe these peculiar oscillations the instrument must have a very high resolution. Thus, in the case of Si, Ag $K\alpha$ and $t \simeq 5t_s$, the period of peculiar oscillations is $\simeq 2$ μm.

If the dimensions of the X-ray tube focus are greater than the period of peculiar oscillations, these oscillations are not developed on the film.

Finally, we need to consider normal oscillations which are due to interference of waves belonging to different branches of the dispersion surface, that is the *Pendellösung* effect. In this case, as usual, the intensity oscillates with increase of t. However, the period of oscillation changes with x.

We consider now what principal differences from Kato's diffraction pattern arise in this region. Firstly, the width of the diffraction region is about $2x_+$ (see previous section). With increase in thickness it gradually increases, not proportionally to t, but more rapidly, until it reaches the dimensions determined by the Kato theory. After that the width of the diffraction region becomes proportional to t.

Secondly, the relationship between the amplitudes of interfering waves changes, which again leads to worsening of the contrast when t is close to t_s.

Thirdly, the geometry of the fringes changes – they are more bent towards the focus region. To demonstrate this let us consider again the central part of the interference pattern, *i.e.* the region $|x| \ll x_+$. In this case the interference points are determined by (5.7) and the phase difference (from which the constant term $\pi/2$ is subtracted) by (5.8). Since in this case $t > t_s$, the phase difference decreases with increase in x, this decrease being the more rapid the closer t is to t_s.

As $|x|$ grows, the tendency of fringes to form V shapes towards region IV increases. This is easy to see in Fig. 8(c), where the interference points are seen to 'disperse' more rapidly as x increases. Thereby all the

interference fringes are within the range $|x| < x_+(t)$. We notice that a reverse process takes place in region II; when $|x|$ increases the period of oscillations gradually increases (see Fig. 8a). Thus, region IV is characterized by relatively low 'visibility' of interference fringes, a good resolution occurring only in the centre.

Such a diffraction pattern is shown in Fig. 5, where the region $4t_s < t < 7t_s$ is presented. In the region $4t_s < t < 5·5t_s$ only first maxima in the central part of rather a narrow fringe are resolved. With the increase of t light spots gradually take the form of fringes, which eventually turn into the fringes of the classical *Pendellösung* effect.

6. Conclusion

The results presented in the previous sections clearly show that the interference pattern, developed on the film due to the diffraction of radiation in a crystal, essentially depends not only on the properties of the crystal but also on the distance between the source and the detector. If the source–crystal–film distance is very large or, in other words, $t_s \gg t$, the diffraction pattern reproduces an angular dependence of the reflexion coefficient in the incident plane-wave approximation, the diffraction-pattern dimension increasing proportionally to L in this case. On the other hand, for small L ($t \gg t_s$), the diffraction pattern takes quite another form and, in particular, is independent of L. In the intermediate region ($t \simeq t_s$), the effect of X-ray spherical-wave focusing occurs, which considerably affects the character of the diffraction pattern in the region of transition from the anomalous (large L) to the ordinary (small L) *Pendellösung* effect.

The knowledge of possible interference structures in X-ray topographs from a perfect crystal is necessary for an analysis of the great variety of topographs obtained from crystals with imperfections. Therefore, the results obtained appear to be of not only pure scientific importance but also a practical one. On the other hand, new possibilities arise of using diffraction for investigation of spectral properties of X-ray radiation. Indeed, if in a thick crystal the phenomenon of focusing is used along with the Borrmann effect, one may obtain highly resolved spectral decomposition of incident radiation in a straight beam.

In conclusion, it should be noted that the analysis performed corresponds to the situation when radiation falls on the crystal directly from the focus of an X-ray tube.

Therefore, in order to observe Kato's type of interference pattern, the distance L should be extremely small. However, in practice, the interference pattern is observed by another experimental arrangement, when the source–crystal distance is not small but a narrow slit is placed near the entrance surface of the crystal.

Obviously, the slit itself may be regarded as a source, when its dimension $a \simeq \lambda$. However, such a condition is never satisfied for X-rays. In this connection a consistent analysis of the slit role in forming the interference pattern, with an account of source–crystal–film distance, is of interest.

References

AFANAS'EV, A. M. & KOHN, V. G. (1977). *Fiz. Tverd. Tela,* **19,** 1775–1783.

ARISTOV, V. V. & POLOVINKINA, V. I. (1978). *Acta Cryst.* A**34,** S227.

ARISTOV, V. V., POLOVINKINA, V. I., SHMYT'KO, I. M. & SKULAKOV, E. V. (1978). *Pis'ma Zh. Eksp. Teor. Fiz.* **28,** 6–9.

BORN, H. & WOLF, E. (1964). *Principles of Optics.* New York: Pergamon Press.

EWALD, P. P. (1917). *Ann. Phys.* **54,** 519–597.

HART, M. & MILNE, A. D. (1968). *Phys. Status Solidi,* **26,** 185–189.

JEFFREYS, H. & SWIRLES, B. (1966). *Method of Mathematical Physics.* Cambridge Univ. Press.

KATO, N. (1961). *Acta Cryst.* **14,** 526–533, 627–636.

KATO, N. (1968). *J. Appl. Phys.* **39,** 2225–2230, 2231–2237.

KATO, N. & LANG, A. R. (1959). *Acta Cryst.* **12,** 787–794.

KOHN, V. G. (1979). *Kristallografiya,* **24,** 712–719.

KOZMIK, V. D. & MIKHAILYUK, I. P. (1978). *Ukr. Fiz. Zh. (Ukr. Ed.),* **23,** 1570–1571.

PINSKER, Z. G. (1978). *Dynamical Scattering of X-rays in Perfect Crystals.* Heidelberg, London, New York: Springer Verlag.

Restrictions in the Arrangement of Molecular Sheets in CdI₂ and PbI₂ Polytypes

BY M. A. WAHAB AND G. C. TRIGUNAYAT

Department of Physics and Astrophysics, University of Delhi, Delhi 110007, India

Abstract

Based on the observations that in the Zhdanov symbols of the known CdI₂ and PbI₂ structures the occurrence of number 3 is far less frequent than the occurrence of numbers 1 and 2 and numbers greater than 3 do not occur at all, a review of these structures has been made. Empirical rules have been evolved, which help in drastically cutting down the number of possible structures of a given polytype and thus considerably facilitate the process of its crystal-structure determination.

Introduction

The layered compounds CdI₂ and PbI₂ are known to be rich in polytypism. Over 260 polytypes of the former and 50 polytypes of the latter have been reported, of which the crystal structures of 90 and 15, respectively, have been determined. An examination of the known structures, listed in Tables 1 and 2, reveals that their Zhdanov symbols rarely contain the number 3. This has led to the formulation of a useful empirical guideline, using which the number of probable structures for a given polytype is drastically reduced.

The nature of the arrangement of molecular sandwiches in the known structures of CdI₂ and PbI₂

The analysis of the structures of CdI₂ and PbI₂ crystals (Tables 1 and 2), grown by various techniques (from solution, melt, vapour and gel) and numbering 105 in all, shows that they are made up of combinations of different types of molecular sandwiches, with each sandwich consisting of a sheet of cadmium atoms nested between two sheets of iodine atoms. All sandwiches are geometrically equivalent but can have six possible orientations, with three belonging to a cyclic group, *viz* $A\gamma B$, $B\alpha C$ and $C\beta A$ and three to an anticyclic group, *viz* $B\gamma A$, $C\alpha B$ and $A\beta C$. The smallest polytype 2*H* is formed by a periodic repetition of any of the above six sandwiches. The second smallest polytype 4*H* ($A\gamma B$ $C\alpha B$ ...) contains sandwiches from alternate groups. The higher polytypes consist of various combinations of sandwiches from the two groups.

Out of the crystal structures listed in Tables 1 and 2, the existence of three structures, *viz* 6*H*₂ and 32*H*₁ of CdI₂ and 6*R* of PbI₂, is doubtful for the following reasons. (*a*) Although the polytypes 6*H*₂ and 6*R* have been reported by Pinsker & co-workers (Pinsker, 1941; Pinsker, Tatarinova & Novikova, 1943), and the poly-